Electronic Supplementary Information

NiCoP Nanoclusters-Anchored Porous $Ti_3C_2T_x$ Monolayer as High Performance Hydrogen Evolution Reaction Electrocatalysts.

Sung M. Kang [a, †], Minjun Kim[b, †], Jeong Bok Lee[a], Shiyu Xu[a], N. Clament Sagaya Selvam[a], Pil J. Yoo [a, b,]*

[a] School of Chemical Engineering, Sungkyunkwan University (SKKU), Suwon 16419, Republic of Korea.

[b] SKKU Advanced Institute of Nanotechnology (SAINT), Sungkyunkwan University (SKKU), Suwon 16419, Republic of Korea.

† Both authors contributed equally to this work.

* Corresponding authors: pjyoo@skku.edu

List of Figures

List of Tables

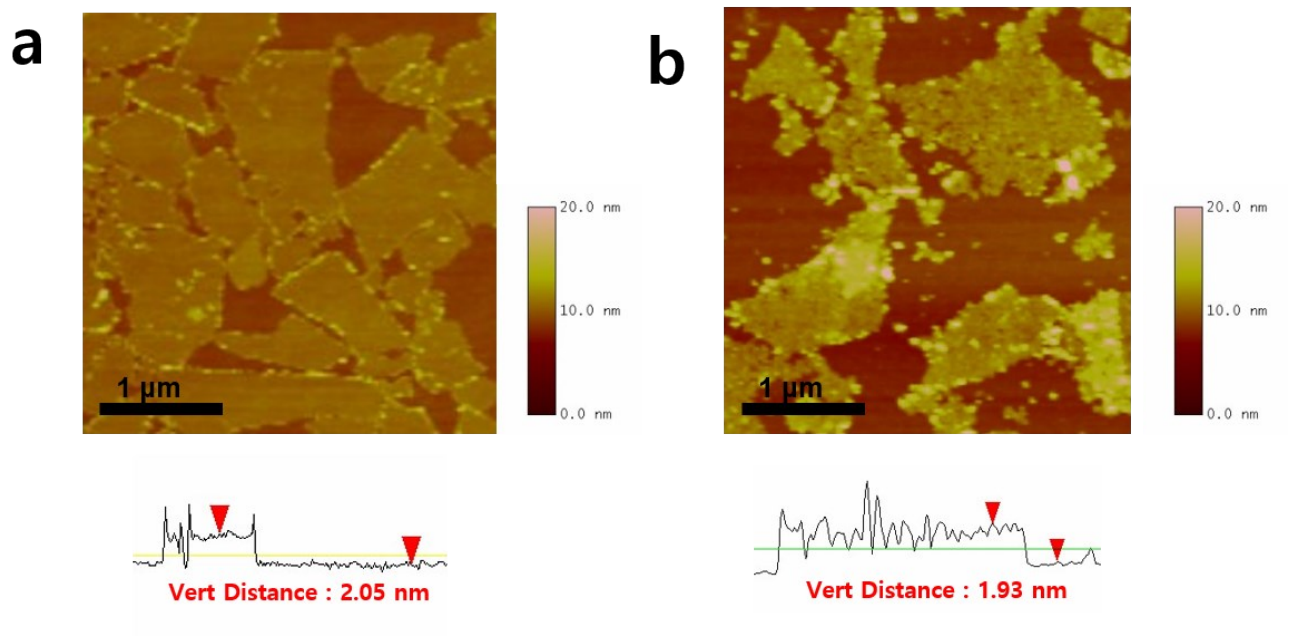

Figure S1. AFM images of the (a) pristine $Ti_3C_2T_x$ and (b) P-$Ti_3C_2T_x$ nanosheets.

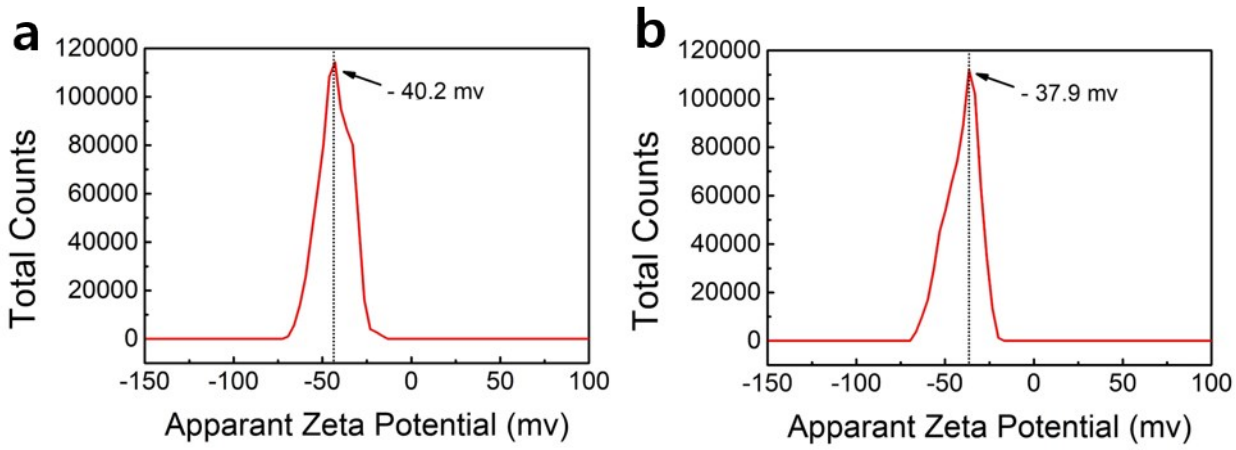

Figure S2. Comparison of zeta-potential values of (a) pristine $Ti_3C_2T_x$ and (b) P-$Ti_3C_2T_x$ nanosheets.

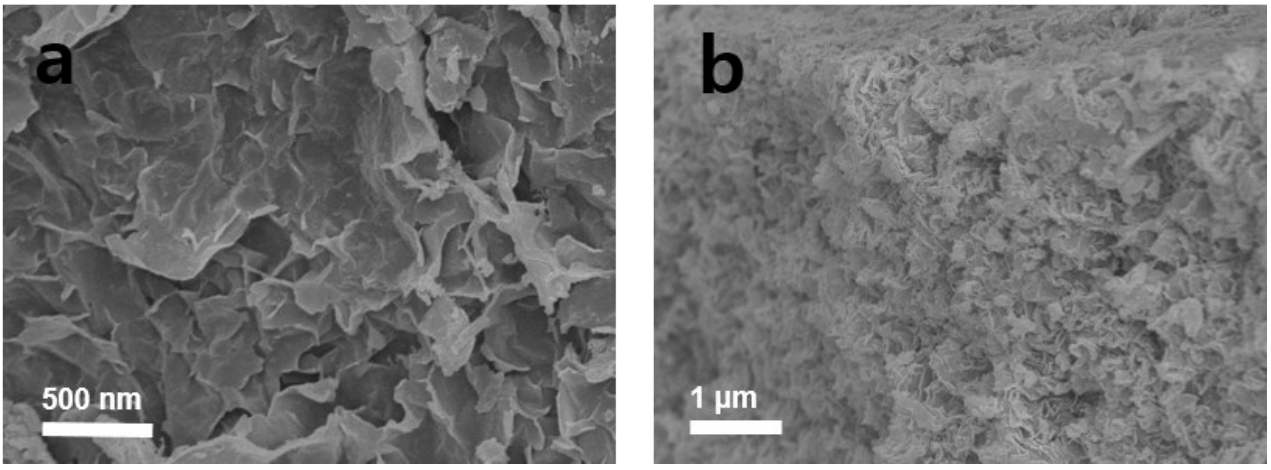

Figure S3. SEM images of (a) P-$Ti_3C_2T_x$@$NiCo(OH)_2$ precursor and (b) P-$Ti_3C_2T_x$@NiCoP 3D nanostructure.

a

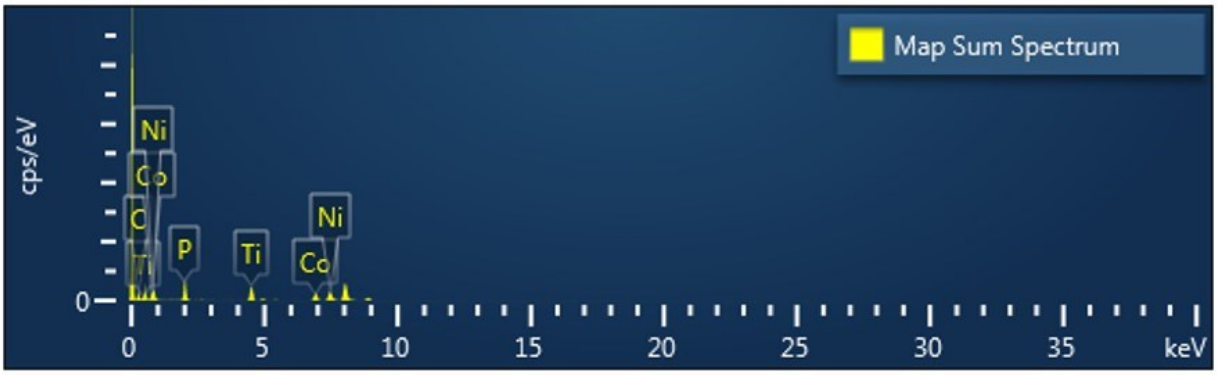

b

Element	Absorption Correction	Weight %	Atomic %
C	1	15.61	40.16
P	1	26.52	26.46
Ti	1	24.77	15.98
Co	1	15.17	7.95
Ni	1	17.94	9.44
Total :		100.00	100.00

Figure S4. (a) Energy dispersive X-ray spectroscopy (EDS) of P-$Ti_3C_2T_x$@NiCoP and (b) its elemental composition.

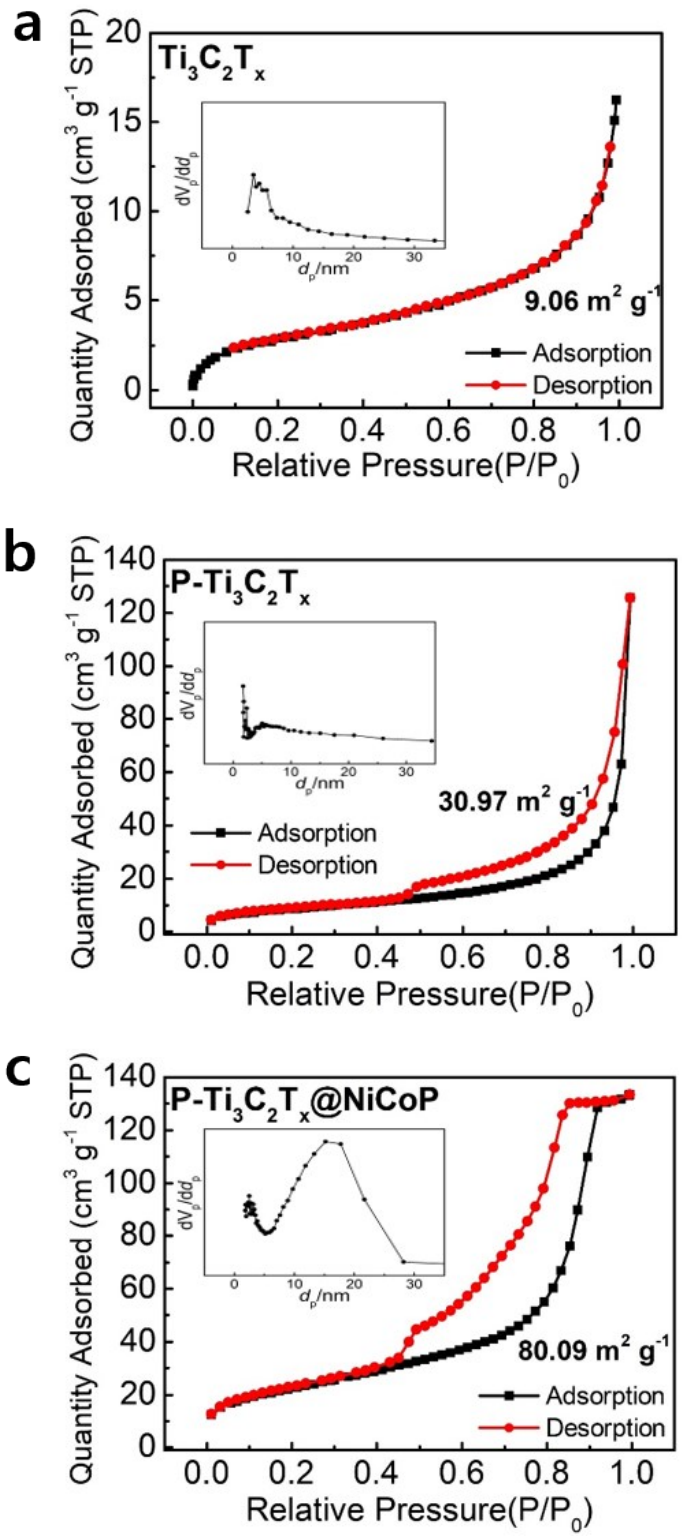

Figure S5. Nitrogen adsorption-desorption isotherms of (a) $Ti_3C_2T_x$, (b) P-$Ti_3C_2T_x$, and (c) P-$Ti_3C_2T_x$@NiCoP 3D nanostructures**.**

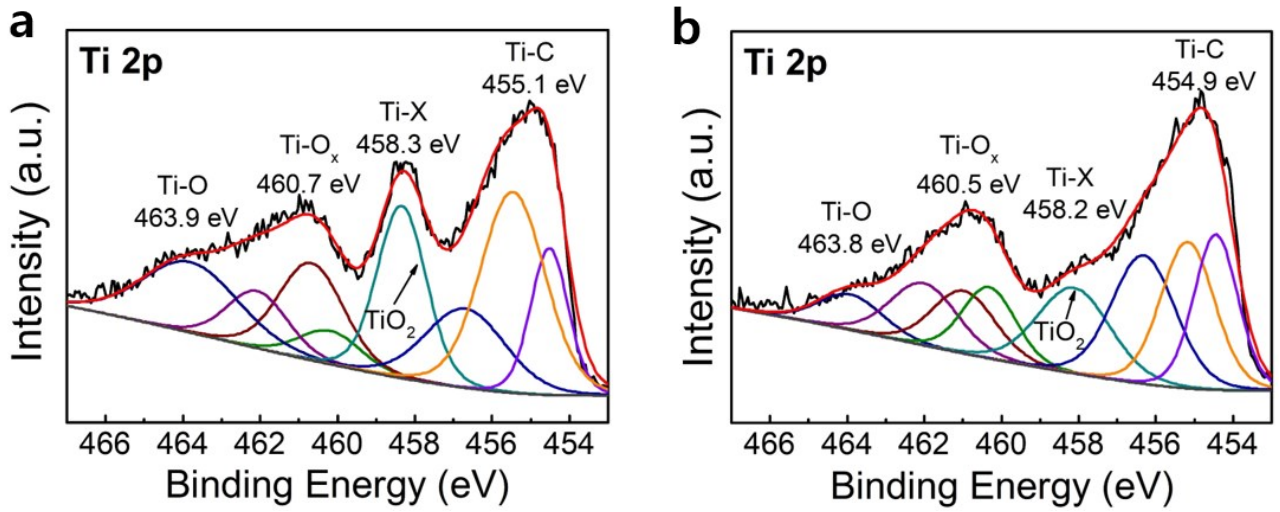

Figure S6. High-resolution XPS spectra of (a) Ti 2p for P-$Ti_3C_2T_x$, and (b) Pristine $Ti_3C_2T_x$ nanosheets.

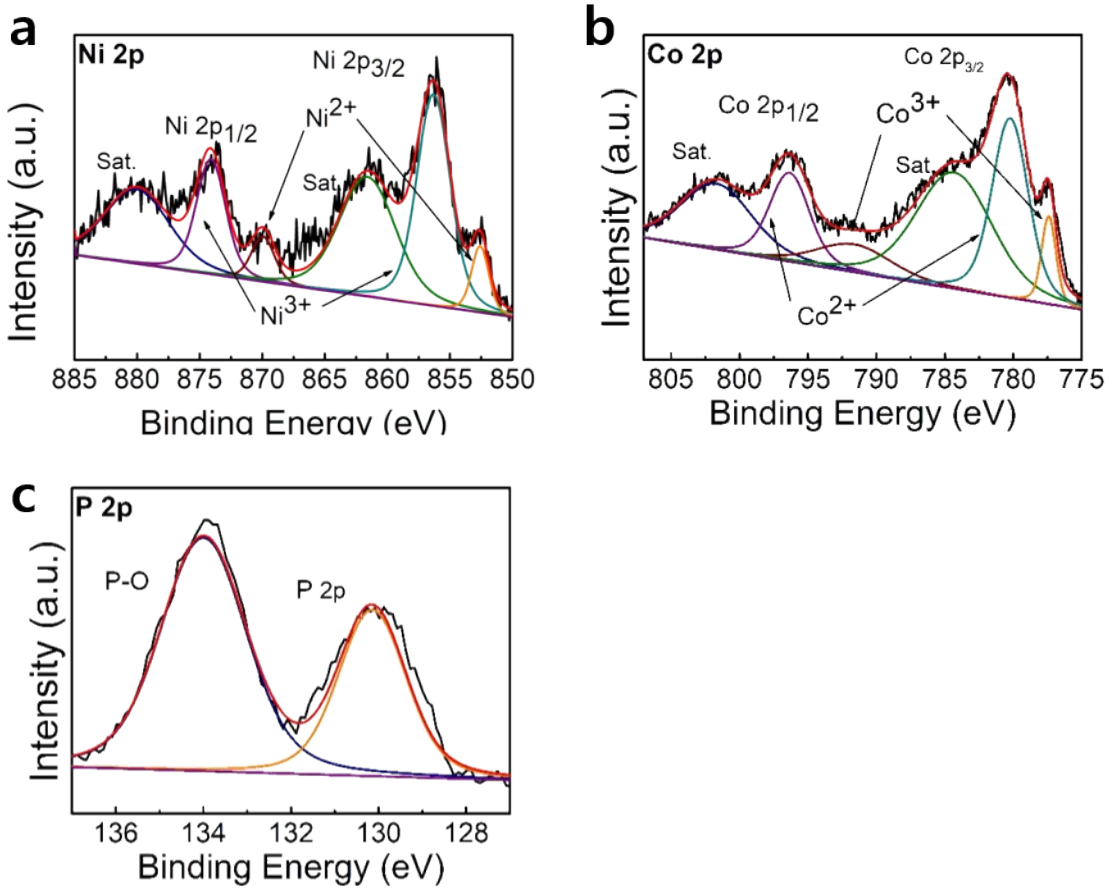

Figure S7. High-resolution XPS spectrum of (a) Ni 2p, (b) Co 2p, and (c) P 2p for pure NiCoP.

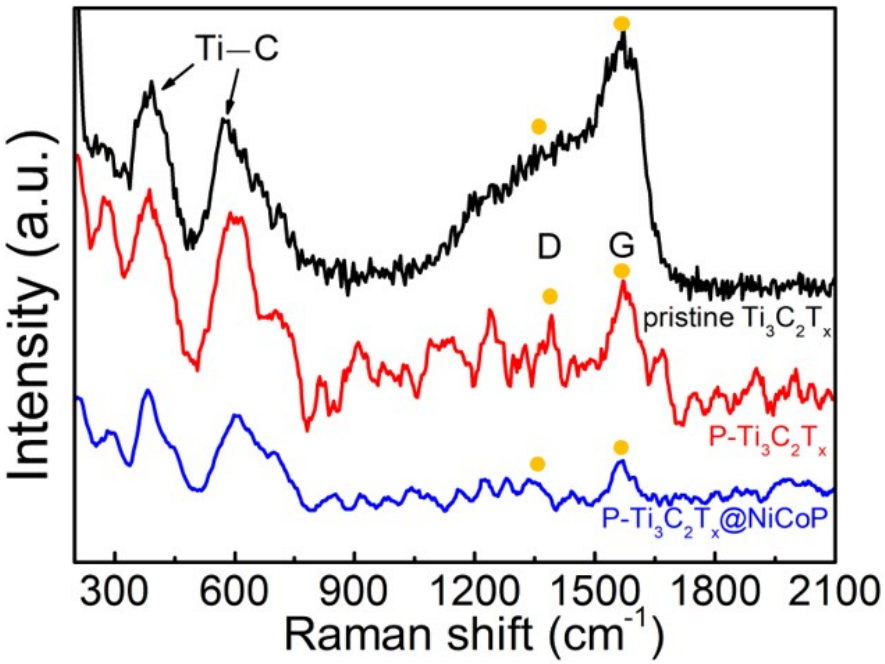

Figure S8. Comparison of Raman spectra of pristine $Ti_3C_2T_x$ (black, top), P-$Ti_3C_2T_x$ (red, middle), and P-$Ti_3C_2T_x$@NiCoP 3D nanostructures (blue, bottom).

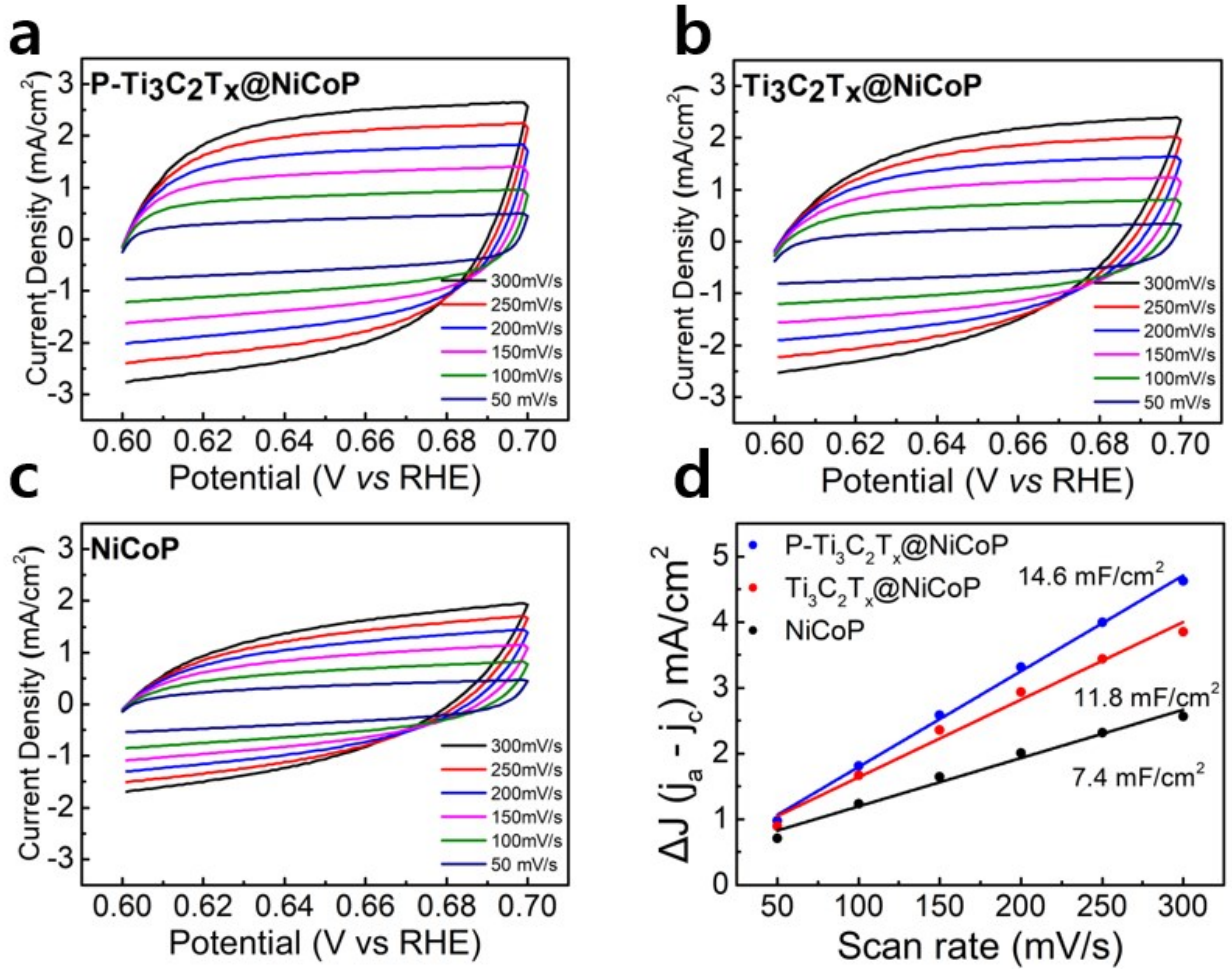

Figure S9. Cyclic voltammograms measured in non-Faradaic region of (a) P-$Ti_3C_2T_x$@NiCoP, (b) $Ti_3C_2T_x$@NiCoP, and (c) NiCoP electrodes at various scan rates for different catalysts in 0.5 M H_2SO_4. (d) Plots of current density differences (Δj) against the scan rates at 0.65 V vs. RHE, where Δj is the difference between anodic and cathodic current densities in CV curves at different scan rates.

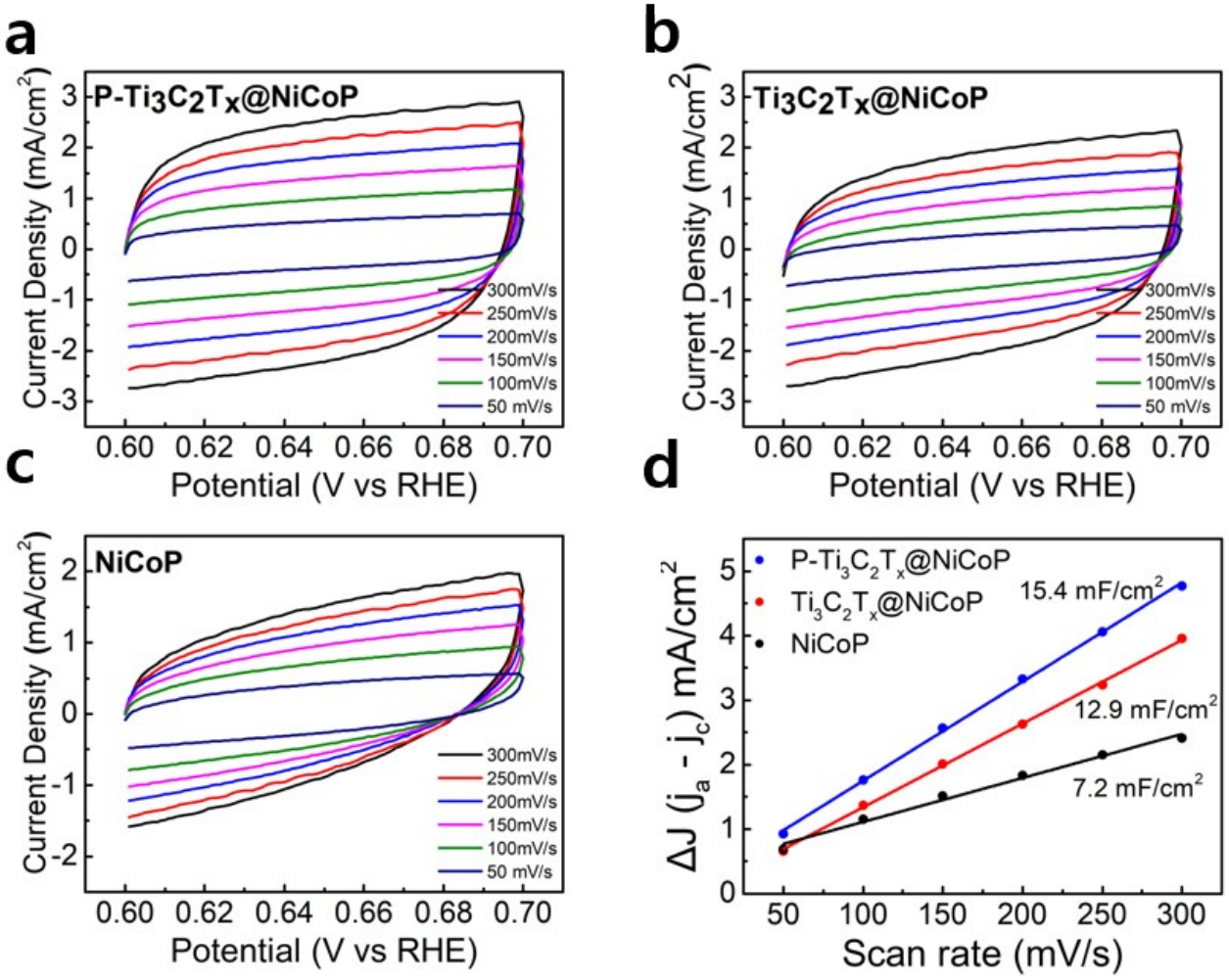

Figure S10. Cyclic voltammograms measured in non-Faradaic region of (a) P-$Ti_3C_2T_x$@NiCoP, (b) $Ti_3C_2T_x$@NiCoP, and (c) NiCoP electrodes at various scan rates for different catalysts in 1 M KOH. (d) the plots of current density differences (Δj) against scan rates at 0.65 V vs. RHE, where Δj is the difference between anodic and cathodic current densities in CV curves at different scan rates.

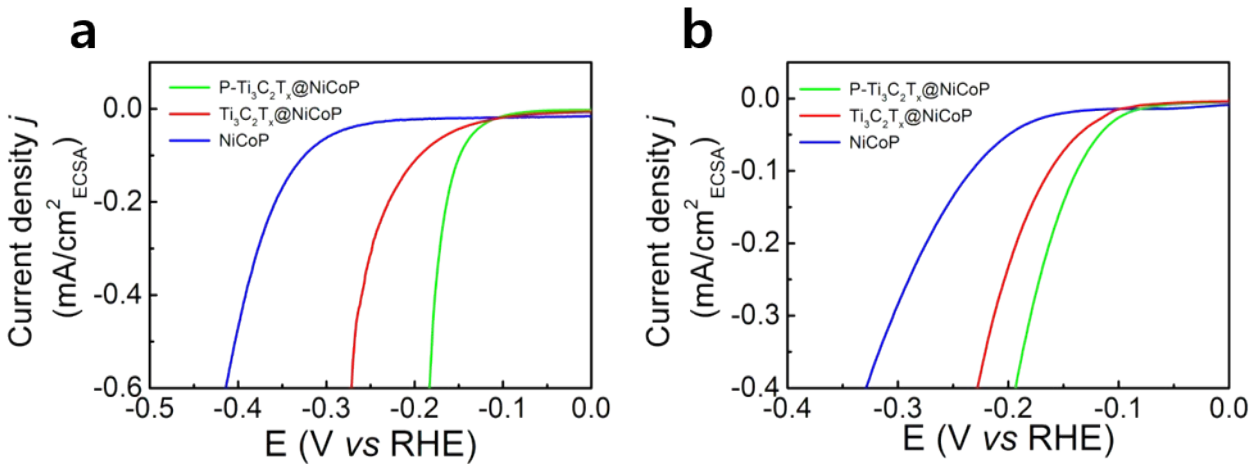

Figure S11. ECSA-normalized HER polarization curves evaluated under (a) 0.5 H_2SO_4 and (b) 1.0 M KOH condition for various catalysts. Note that presented HER polarization curves in Fig. 4a and Fig. 5a were normalized by ECSA values as summarized in Table S3 and S4 to compare the intrinsic catalytic activity of various samples.

Table S1. Comparison of atomic ratio normalized by Ti for various samples obtained from ICP-OES measurements.

Sample	Ti/Ti	Ni/Ti	Co/Ti	P/Ti
P-$Ti_3C_2T_x$@NiCoP	1	0.47	0.86	1.43
$Ti_3C_2T_x$@NiCoP	1	0.31	0.72	1.26

Table S2. Comparison of the HER performance of P-$Ti_3C_2T_x$@NiCoP with other non-noble metal based electrocatalysts reported before.

Catalysts	Overpotential (mV) $\eta_{10\ mA\ cm-2}$	Tafel slope (mV dec^{-1})	Electrolyte	Reference
P-$Ti_3C_2T_x$@NiCoP	**101** **115**	**69** **76**	**1 M KOH** **0.5 M H_2SO_4**	**This work**
NiCo2O4/NiCoP	198	91	1 M KOH	[1]
NiCoP/CNF	130	83	1 M KOH	[2]
NiCoP NPs/Ti,	97	50	1 M KOH	[3]
NiCoP–CoP/NF	73	91.3	1 M KOH	[4]
$NiCo_2O_4$/Ni_2P/NAs	141 116	86 37	1 M KOH 0.5 M H_2SO_4	[5]
Ni_5P_4–NiP_2/NF	92	52.8	1 M KOH	[6]
NiFe LDH@NiCoP	120	88.2	1 M KOH	[7]
S-NiCoP NW/CFP	102	63.3	1 M KOH	[8]
NiCoP-C(TPA)/NF	78 94	73.4 81.1	1 M KOH 0.5 M H_2SO_4	[9]
O-NiCoP/Ni_2P	58	68.8	1 M KOH	[10]
O-doped Co_2P	101	69.4	1 M KOH	[11]
CoP-MOF	34 27	63 56	1 M KOH 0.5 M H_2SO_4	[12]
$NiPS_3$/Ni_2P	85	82	1 M KOH	[13]
CoP/NiCoP/NC	75 60	58 60	1 M KOH 0.5 M H_2SO_4	[14]
CoP/NiCoP	121 90	65 68	1 M KOH 0.5 M H_2SO_4	[15]

Table S3. Summary of the HER performance, C_{dl} and ECSA of various electrocatalysts measured in 0.5 M H_2SO_4.

Catalysts	$\eta_{10mA\ cm^{-2}}$ (mV)	Tafel slopes (mV dec^{-1})	C_{dl} (mF cm^{-2})	ECSA
P-$Ti_3C_2T_x$@NiCoP	115	76	7.4	185
$Ti_3C_2T_x$@NiCoP	145	85	11.8	295
NiCoP	178	125	14.6	365

Table S4. Summary of the HER performance, C_{dl} and ECSA of various electrocatalysts measured in 1.0 M KOH.

Catalysts	$\eta_{10mA\ cm^{-2}}$ (mV)	Tafel slopes (mV dec^{-1})	C_{dl} (mF cm^{-2})	ECSA
P-$Ti_3C_2T_x$@NiCoP	101	69	7.2	180
$Ti_3C_2T_x$@NiCoP	121	78	12.9	322.5
NiCoP	170	101	15.4	385

Note: ECSA for HER was determined based on the specific capacitance (C_s) of the NiCoP (0.040 mF cm^{-2}) from the literature and the obtained ECSA values of the catalysts were normalized by the ECSA value of NiCoP. [16].

References

[1] W. Jin, J. Chen, H. Wu, N. Zang, Q. Li, W. Cai and Z. Wu, *Catalysis Science & Technology*, 2020, **10**, 5559-5565.

[2] S. Surendran, S. Shanmugapriya, A. Sivanantham, S. Shanmugam and R. Kalai Selvan, *Advanced Energy Materials*, 2018, **8**, 1800555.

[3] C. Wang, J. Jiang, T. Ding, G. Chen, W. Xu and Q. Yang, *Advanced Materials Interfaces*, 2016, **3**, 1500454.

[4] H. Liu, X. Ma, H. Hu, Y. Pan, W. Zhao, J. Liu, X. Zhao, J. Wang, Z. Yang and Q. Zhao, *ACS applied materials & interfaces*, 2019, **11**, 15528-15536.

[5] Q. Wang, H. Wang, X. Cheng, M. Fritz, D. Wang, H. Li, A. Bund, G. Chen and P. Schaaf, *Materials Today Energy*, 2020, **17**, 100490.

[6] S. Liu, C. Hu, C. Lv, J. Cai, M. Duan, J. Luo, J. Song, Y. Shi, C. Chen and D. Luo, *International Journal of Hydrogen Energy*, 2019, **44**, 17974-17984.

[7] H. Zhang, X. Li, A. Hähnel, V. Naumann, C. Lin, S. Azimi, S. L. Schweizer, A. W. Maijenburg and R. B. Wehrspohn, *Advanced Functional Materials*, 2018, **28**, 1706847.

[8] Y. Qi, L. Zhang, L. Sun, G. Chen, Q. Luo, H. Xin, J. Peng, Y. Li and F. Ma, *Nanoscale*, 2020, **12**, 1985-1993.

[9] S. Sirisomboonchai, S. Li, A. Yoshida, S. Kongparakul, C. Samart, Y. Kansha, X. Hao, A. Abudula and G. Guan, *Catalysis Science & Technology*, 2019, **9**, 4651-4658.

[10] Y. Wen, J. Qi, D. Zhao, J. Liu, P. Wei, X. Kang and X. Li, *Applied Catalysis B: Environmental*, 2021, **293**, 120196.

[11] T. L. L. Doan, D. T. Tran, D. C. Nguyen, H. T. Le, N. H. Kim and J. H. Lee, *Applied Catalysis B: Environmental*, 2020, **261**, 118268.

[12] T. Liu, P. Li, N. Yao, G. Cheng, S. Chen, W. Luo and Y. Yin, *Angewandte Chemie*, 2019, **131**, 4727-4732.

[13] Q. Liang, L. Zhong, C. Du, Y. Luo, J. Zhao, Y. Zheng, J. Xu, J. Ma, C. Liu and S. Li, *ACS nano*, 2019, **13**, 7975-7984.

[14] R. Boppella, J. Tan, W. Yang and J. Moon, *Advanced Functional Materials*, 2019, **29**, 1807976.

[15] X. Liu, S. Deng, D. Xiao, M. Gong, J. Liang, T. Zhao, T. Shen and D. Wang, *ACS applied materials & interfaces*, 2019, **11**, 42233-42242.

[16] S. Sirisomboonchai, S. Li, A. Yoshida, S. Kongparakul, C. Samart, Y. Kansha, X. Hao, A. Abudula and G. Guan, *Catalysis Science & Technology,* 2019, **9**, 4651.